JOURNAL OF MATERIALS SCIENCE 20 (1985) 1807–1814

Iron impurities in Si_3N_4 processing

C. E. BOULDIN, E. A. STERN, M. S. DONLEY*, T. G. STOEBE*
*Department of Physics, FM-15 and *Department of Materials Science and Engineering, FB-10, University of Washington, Seattle, Washington 98195, USA*

The atomic environment of iron impurities is investigated during the processing cycle of reaction-bonding silicon nitride (RBSN). Several analysis techniques are utilized, including X-ray photoelectron spectroscopy (XPS), extended X-ray absorption fine structure (EXAFS), and electron spin resonance (ESR), to examine iron impurities in the starting silicon powder, in sintered silicon compacts, and in RBSN materials. Results indicate that iron impurities in as-received metallurgical grade silicon powder are incorporated in the silicon bulk as a highly distorted $FeSi_2$ compound. No surface iron or iron-based particulate is observed in the starting material. Upon sintering, the iron environment becomes an ordered $FeSi_2$ structure. In the RBNS material, the $FeSi_2$ structure is again distorted, as observed by both EXAFS and ESR.

1. Introduction

Reaction-bonded silicon nitride (RBSN) is currently being considered in a variety of high performance materials applications because of its excellent corrosion resistance and good thermal shock and creep resistance. However, RBSN is a brittle material whose mechanical properties are affected to a large extent by processing variables and by starting silicon powder purity. Despite extensive research on the reaction of Si(s) and N_2(g) [1–7], the reaction kinetics are not completely understood. Introducing impurities into this reaction significantly complicates the picture. While the macroscopic effects of an impurity can be observed, it is difficult to correlate these effects with kinetic processes atributable to a specific impurity.

Iron is frequently added to silicon powder in the production of RBSN because it is generally believed to accelerate the nitridation reaction, although the specific mechanism responsible for this acceleration is unclear. The role of iron in silicon nitride processing has been discussed by many investigators. One theory [8] attributes the nitridation acceleration to iron–oxygen interactions, where iron induces volitization of the native oxide layer on the silicon particles. A variation on this theory [9, 10] suggests that iron reacts with SiO and O_2 to form FeO, thereby lowering the O_2 partial pressure. Another theory [11] attributes the accelerated nitridation to the formation of an $FeSi_x$ melt which promotes liquid phase β-Si_3N_4 growth. Some investigators [12, 13] have concluded that while iron modifies the native SiO_2 layer on the silicon, the iron must first form a $FeSi_x$ liquid before it becomes effective.

This paper presents the results of an interdisciplinary study of the location of iron impurities during the processing cycle of reaction-bonded silicon nitride. Iron impurities are examined in starting silicon powder, in sintered silicon compacts, and in reaction-bonded silicon nitride material. The study involves the use of several analysis techniques, namely X-ray photoelectron spectroscopy (XPS), extended X-ray absorption fine structure (EXAFS), and electron spin resonance (ESR), and concentrates on data obtained from an as-received metallurgical grade silicon powder.

2. Experimental details

Two silicon powders, designated S3 and S5, were investigated; a spectrographic analysis of the impurity content of these powders is presented in Table I. The S3 powder was as-received metallurgical grade silicon powder and contained 0.63% iron by weight, as determined by two different

0022–2461/85 $03.00 + .12

TABLE I Sample impurity content. Plasma spectrographic analysis of imprints, given in ppm by weight*

Element	Concentration (ppm)		Detection limit
	S3	S5	
Al	3780	3820	37.5
Ca	518	498	2.5
C†	1400	1400	100
Fe	6310	15 900	7.5
Mn	198	426	0.75
Ti	410	418	1.5

*Analysis performed by AMTEST, Inc. Seattle, Washington.
†Analysis using Leco Furnace apparatus.

TABLE II Results of X-ray diffraction of RBSN samples. Components of samples in % of weight, ± 25% accuracy

Component	Sample	
	S3	S5
α-Si_3N_4	64.6	67.4
β-Si_3N_4	21.5	31.7
Si_2ON_2	0.9	0.5
Si	11.5	0.7
$FeSi_x$	1.3	2.2
SiO_2	0.2	0.3
α/β	3.33	2.33
Density	2.00	2.26

wet chemical techniques. S5 was prepared by doping the S3 powder with Fe_2O_3 (haematite) to yield a total iron content of approximately 1.6% by weight. All silicon powders had an average particle size of 5 μm and were purchased from Union Carbide, Inc.

Specimens were prepared by dry-pressing silicon powders of each composition into pellets of 1.27 cm diameter under a pressure of 6.89 MPa. (This pressure was selected because it produced pellets of low density which, although somewhat fragile, could be handled successfully during processing.) The pellets were then processed by one of two methods: (1) nitrided only, or (2) sintered and then nitrided. The sintering was done in vacuum (10^{-5} torr) for 4 h at 1100° C in a chamber heated by molybdenum elements. The nitriding cycle followed a procedure outlined by Mangels [14], which utilized the thermal conductivity of a H_2–He background gas. The pellets were placed in a chamber and heated to 800° C in vacuum (10^{-5} torr), and the chamber was then backfilled with 66% nitrogen, 4% hydrogen, and 30% helium. The nitridization utilized a nitrogen demand cycle in which the heating rate was coupled to nitrogen intake. The process required 12 days for completion and ended with a nitrogen demand of 0.5 litre h^{-1} at 1400° C.

To investigate the bulk composition of the RBSN material, X-ray diffraction analysis was applied in the manner outlined by Mencik and Short [15]. Powder specimens were irradiated using a Cu$K\alpha$ X-ray source with a graphite monochromator, and the diffraction patterns were recorded and analysed for the presence of α-Si_3N_4, β-Si_3N_4, Si, SiO_2, Si_2ON_2, and iron silicides. The phase composition of the as-received metallurgical grade powder, S3, is contrasted with the Fe_2O_3-doped powder, S5, in Table II, which also reports the α/β ratio and the density of the RBSN product.

ESR spectra were taken at room temperature and at 77 K using powdered samples in a Varian model E3 spectrometer. DPPH was used as a primary ESR standard and polycrystalline $CuSO_4 \cdot 5H_2O$ was used as a secondary standard. EXAFS measurements were made on powdered samples by the fluorescence method using a soller slit and manganese filter [16]: the measurements were made at the Stanford Synchroton Radiation Laboratory in beamline IV at temperatures of 10, 80 and 300 K. XPS was performed at the Perkin-Elmer Surface Science Division Analytical Laboratory using a PHI model 560 microprobe in the ESCA mode.

3. Results and discussion

3.1. XPS

The XPS spectrum determined for a sample of the as-received metallurgical grade silicon powder S3 is shown in Fig. 1. These results are presented in a scan at the "surface" of the powder (Fig. 1a) and a scan after sputtering to a "depth" of 20 nm (Fig. 1b). Here, "surface" is used to indicate the top-most layer of particles and "depth" is used to indicate a distance downward from this top layer of particles. The average particle size is 5 μm and the analysis area is approximately 3 mm diameter. Neither XPS scan indicates the detectable presence of iron in the as-received powder. However, the presence of a "native oxide" coating on the silicon particles is indicated by the reduction in the oxygen peak between the surface and the 20 nm depth.

If iron were present as particulate, whether distributed as a few large particles or as many very small particles, or if the iron were located within

a few lattice spaces of the surface of the silicon particles, iron would be detected in this analysis. The detection limit for iron in the PHI Model 560 Microprobe is 0.1 at % with an accuracy of ± 10%. The as-received powder is known to contain 6300 $\mu g\, g^{-1}$ or 0.18 at % iron, which is close to the detection limit. However, iron has successfully been detected at or near the detection limit in other analyses by the Perkin-Elmer Analytical Group. In addition, if the iron were concentrated at the surface of the silicon particles, its concentration would be greatly increased above the average level. Therefore, this analysis provides strong evidence that a substantial portion of the iron impurities present in commercial silicon powder resides in the bulk of the sample.

3.2. EXAFS

EXAFS consists of the oscillatory structure in the X-ray absorption just above the absorption edge. The "edge" occurs when an incident photon has sufficient energy to ionize the central atom and eject a photoelectron. The fine structure is due to the presence of surrounding atoms which scatter the outgoing photoelectron and give rise to interference. The detailed shape of the fine structure is sensitive to the arrangement of the surrounding atoms, and the EXAFS oscillations can be analysed to determine the atomic structure in the material. The amplitude of the oscillations gives the number and type of neighbouring atoms and the phase of the oscillations determines the atomic distance. The EXAFS can be Fourier transformed to give an effective average radial distribution function about a particular atomic species [16].

The average radial distribution function about the iron impurity in the as-received silicon powder S3 is shown in Fig. 2. The distribution function shows that there is only one major peak in the

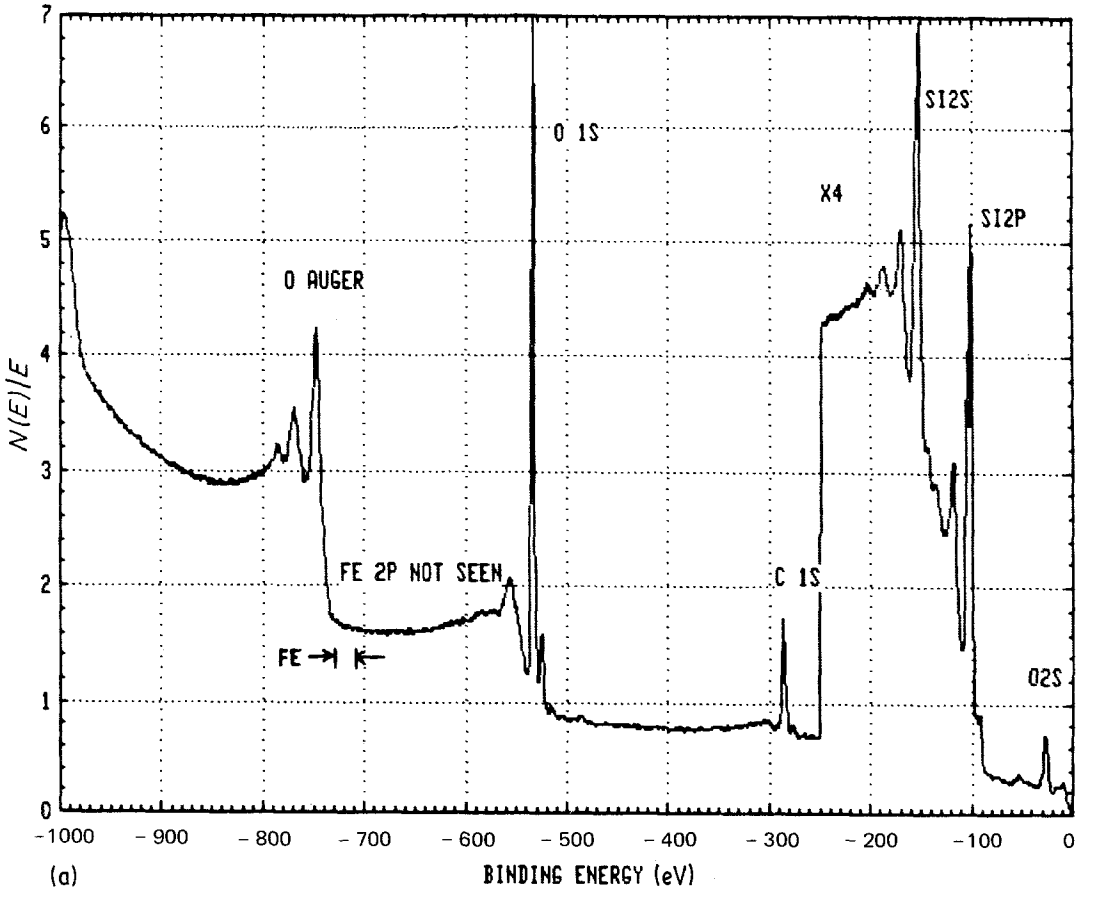

Figure 1 XPS analysis of S3, the as-received metallurgical grade silicon powder. (a) as-received, (b) after 20 nm of the surface has been sputtered away. Note the X 4 scale change at −250 eV.

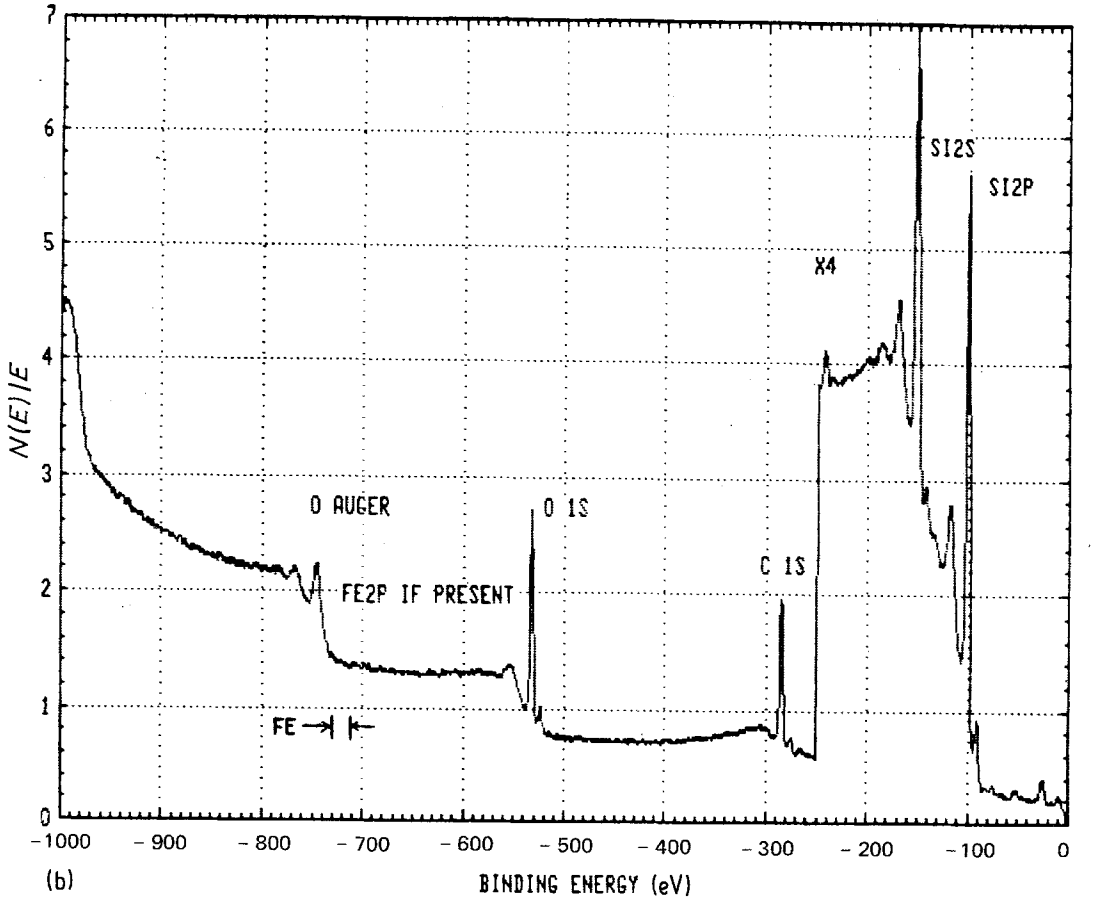

Figure 1 Continued

transform. A detailed analysis of the distribution function shows that the first shell can be modelled by a combination of iron and silicon atoms in a highly disordered $FeSi_2$ structure: this model is verified by the lack of an appreciable temperature dependence of the EXAFS from 10 K to room temperature, indicating that the large disorder was essentially entirely structural. The distribution function also shows that there is no metallic iron present in sample S3, since this would lead to peaks at larger distances.

Fig. 3 shows the radial distribution function about the iron impurity determined in sample S5 after reaction bonding. Again, the distribution function is dominated by a single peak, composed of both iron and silicon atoms. Analysis of the distribution function indicates that the iron is now in a less distorted $FeSi_2$ structure than in the starting powder: this distortion is still greater than in bulk $FeSi_2$.

Details of the structure in the starting silicon powder, the sintered powder (1060° C), and the reaction-bonded silicon nitride are given in Table III for sample S3. Here, N gives the number of nearest iron or silicon neighbours surrounding each iron atom. R is the distance between the iron atom and the neighbouring silicon or iron atom, and $\Delta\sigma^2$ is the disorder in the shell distance. The interpretation of these results is that the iron starts out in a highly disordered $FeSi_2$ structure and that as the material is sintered, the $FeSi_2$ structure anneals into an ordered form. After reaction bonding, the iron disilicide is again distorted from the structure of a bulk $FeSi_2$ crystal but less so than in the starting material. The distortion in the reaction-bonded form is interpreted to mean that the $FeSi_2$ has a large surface-to-volume ratio. The distortion at the interface propagates inward only several atomic lengths so that the final form of the $FeSi_2$ must be such that each iron is within several interatomic dimensions of the interface. No evidence is seen for the formation of Fe–N compounds.

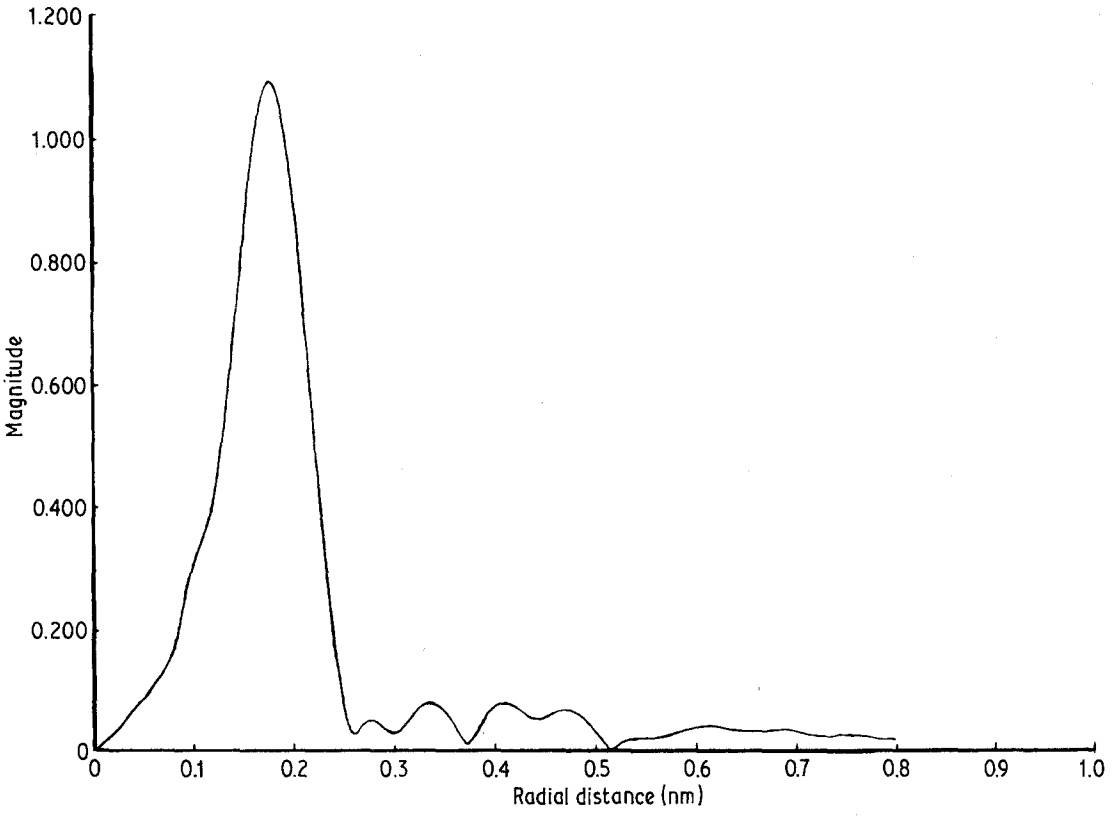

Figure 2 EXAFS Fourier transform indicating the effective average radial distribution function about the iron impurity in the as-received metallurgical grade silicon powder, S3.

3.3. ESR

The ESR spectrum of the as-received silicon powder exhibits a single absorption line, approximately 6.5 G peak-to-peak in width with a g-value of 2.0055 ± 0.0005. This line is consistent in g-value with that produced by silicon dangling bonds [17]. This interpretation implies the absence of paramagnetic iron species in solid solution in the silicon starting material, which is consistent with the low solubility of iron in silicon [18]. The effect of sintering is to reduce the intensity of this absorption line. For a 4 h 1100° C sinter, this peak intensity decreases 90%. No additional absorption lines are observed in the sintered material.

Upon nitridation, two types of ESR signals are observed. First, a very broad single waveform,

TABLE III The iron environment as determined by EXAFS in as-received, metallurgical grade silicon powder (sample S3)

Sample	Si neighbours			Fe neighbours		
	N	R (nm)	$\Delta\sigma^2$ (nm)^2	N	R (nm)	$\Delta\sigma^2$ (nm^2)
Si powder	8	0.238	0.000 10	4	0.272	0.000 10
	± 2.0	± 0.003	± 0.000 05	± 2	± 0.004	± 0.000 05
Sintered Si	9	0.237	0.000 03	4.0	0.279	0.000 03
	± 1.5	± 0.003	± 0.000 008	± .5	± 0.003	± 0.000 008
Nitrided Si	8	0.233	0.000 09	4.5	0.277	0.000 03
	± 1.5	± 0.003	± 0.000 008	± .5	± 0.003	± 0.000 008
$FeSi_2$	8	0.235		4	0.269	

N is the number of nearest neighbours at the average distance R. The rms disorder about R relative to $FeSi_2$ is $\Delta\sigma^2$ in units of nm^2.

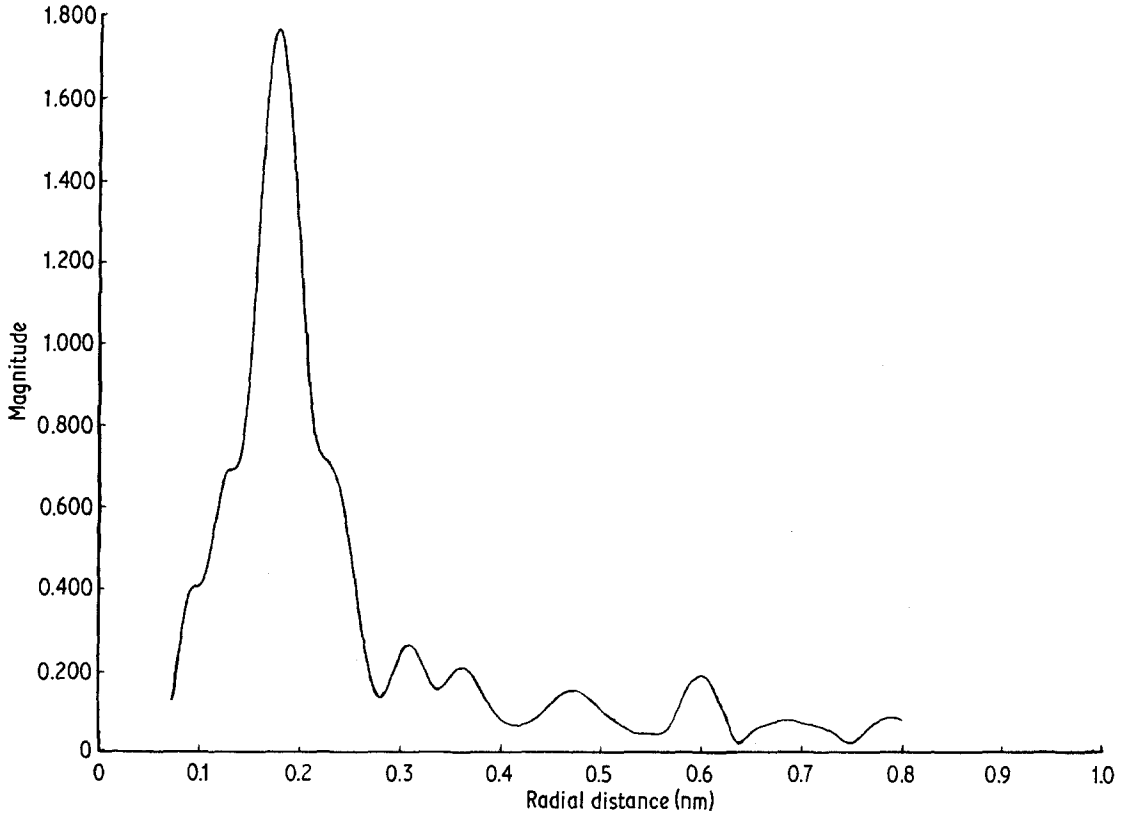

Figure 3 EXAFS Fourier transform indicating the effective average radial distribution function about the iron impurity in the S5 reaction-bonded silicon nitride sample.

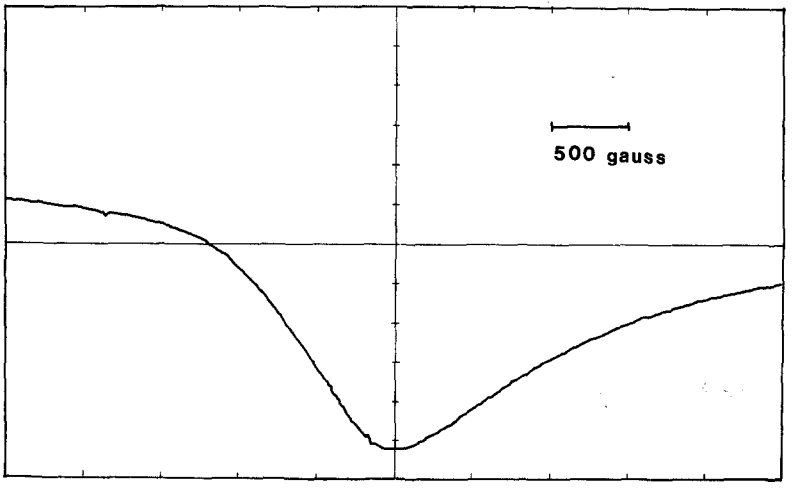

Figure 4 ESR spectrum of the S5 reaction-bonded silicon nitride sample showing the broad single waveform. (Scan width 5000 G.)

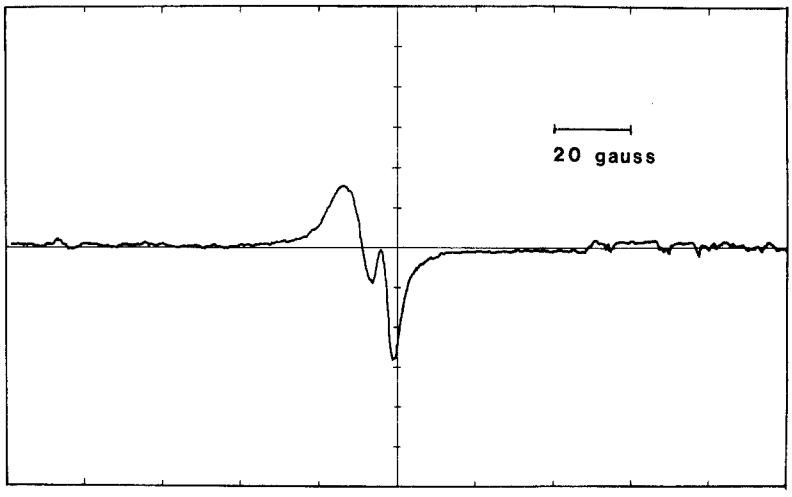

Figure 5 ESR spectrum of the S3 reaction-bonded silicon nitride sample at 77 K showing the two overlapping absorption peaks. (Scan width 200 G.)

unlike the conventional first derivative of the resonance absorption line, is observed. This signal in sample S3 is shown in Fig. 4. This type of waveform is characteristic of Fe^{3+} ions interacting in close proximity with one another. By comparing spectra from a variety of powder compositions, it can be shown that this signal is consistant with that produced by an iron silicide in a highly stressed state, as in the EXAFS result above. Second, a sharp absorption line is seen, approximately 9.5 G peak-to-peak in width, with a g-value close to that of the silicon dangling bond. Inspection of this absorption line at 77 K, shown in Fig. 5, indicates that this waveform is actually two overlapping lines. These absorption lines are very close in g-value, and could be produced by Fe^{3+} in solution in RBSN and/or dangling bonds in Si_3N_4. The multiphase microstructure and high impurity content make it impossible to identify absolutely these lines at this point.

4. Conclusions

The results of this study indicate that the iron impurities in the silicon powder sample S3, the as-received metallurgical grade powder, are incorporated in the silicon bulk. This is confirmed by two independent results: XPS measurements before and after sputtering to a depth of 20 nm give no indication of near-surface iron, and EXAFS measurements indicate that the iron is contained in a highly distorted $FeSi_2$ compound. No evidence of an iron oxide (the likely form if the iron were on the surface) nor of Fe-based particulate (e.g. Fe_3C) is found.

As the sample is heated to temperatures well below those temperatures where reaction bonding with nitrogen becomes appreciable, the iron environment becomes that of an ordered $FeSi_2$ and remains thus until reaction bonding is complete. In the final form, the $FeSi_2$ is again distorted, though less so than in the initial powder, indicating that it has a large interface surface-to-volume ratio. The ESR results are consistent with those from EXAFS, showing a broad waveform which can be explained by the distorted iron environment.

Acknowledgements

The XPS analysis was carried out in cooperation with the Perkin-Elmer Surface Analytical Laboratory, and the authors would like to specifically acknowledge the assistance of the late Thomas E. Brady. This research is supported by the NASA Ceramic Structural Materials Program, Grant NAGW199.

References

1. J. W. EVANS and S. K. CHATTERJI, *J. Phys. Chem.* **62** (1958) 1064.
2. K. J. HUETTINGER, *High Temp. High Pressures* **1** (1969) 221.
3. D. R. MESSIER and P. WONG, *J. Amer. Ceram. Soc.* **56** (1973) 480.
4. A. ATKINSON, P. J. LEATT, A. J. MOULSON and E. W. ROBERTS, *J. Mater. Sci.* **9** (1974) 981.
5. R. HECKINGBOTTOM and R. WOOD, *Surf. Sci.* **36** (1973) 594.
6. A. G. SCHROTT and S. C. FAIN, Jr, *ibid.* **111** (1981) 39.
7. H. M. JENNINGS, *J. Mater. Sci.* **18** (1983) 951.

8. S. M. BOYER and A. J. MOULSON, *ibid.* **13** (1978) 1637.
9. S. LIN, *J. Amer. Ceram. Soc.* **58** (1975) 271.
10. *Idem. Ibid.* **60** (1977) 78.
11. M. MITOMO, *J. Mater. Sci.* **12** (1977) 273.
12. W. FATE and M. MILBERG, *J. Amer. Ceram. Soc.* **61** (1978) 531.
13. S. SHINOZAKI and M. MILBERG, *ibid.* **64** (1981) 382.
14. J. MANGELS, *Amer. Ceram. Soc. Bull.* **60** (1981) 613.
15. Z. MENCIK and M. A. SHORT, "Quantitative Phase Analysis of Synthetic Silicon Nitride by X-ray Diffraction: An Improved Procedure", Ford Motor Co. Technical Report SR-72-98 (1972).
16. E. A. STERN and S. M. HEALD, *Rev. Sci. Instrum.* **50** (1979) 1579.
17. D. HANEMAN, *Phys. Rev.* **170** (1968) 705.
18. F. A. TRUMBORE, *Bell Syst. Tech. J.* **39** (1960) 205.

Received 7 June
and accepted 6 July 1984